



Autoignition of n-heptane in a turbulent co-flowing jet

Tarek Echekki^{a,*}, Samer F. Ahmed^b

^a Department of Mechanical and Aerospace Engineering, North Carolina State University, Raleigh, NC, United States

^b Thermo fluids Group, Department of Mechanical and Industrial Engineering, College of Engineering, Qatar University, P.O. Box 2713, Doha, Qatar



ARTICLE INFO

Article history:

Received 29 March 2015

Revised 12 July 2015

Accepted 13 July 2015

Available online 31 July 2015

Keywords:

Turbulent jet ignition

The one-dimensional turbulence model

Autoignition

ABSTRACT

N-heptane autoignition in turbulent co-flowing jets with preheated air is studied using the one-dimensional turbulence (ODT) model. The simulations are designed to investigate the effects of molecular and turbulent transports on the process of autoignition. Both homogeneous and jet configuration simulations are carried out. The jet configurations are implemented at different jet inlet Reynolds numbers and for two air preheat conditions. Statistics for the cases considered show that, while the onset of autoignition may be delayed by turbulence, the eventual evolution of the volumetric heat release rate indicates that turbulence enhances the post-ignition stages. Since different regions of the mixture can have different ignition delays and may be characterized by one- or two-stage ignition, the autoignition process can be accelerated by ignition kernel propagation or the role of heat dissipation may be reduced through the prevalence of one-stage and two-stage ignitions in different regions of the mixture.

© 2015 The Combustion Institute. Published by Elsevier Inc. All rights reserved.

1. Introduction

Autoignition is an important process for initiating or sustaining combustion in a number of practical devices [1,2]. It is also considered a viable mechanism for flame stabilization in non-premixed systems when either or both the fuel or oxidizer streams are preheated to ignition temperatures [3]. Conditions of ignition are governed by the competition of ignition chemistry with molecular and turbulent transport; and this competition may determine the fate or intensity of the combustion process. In igniting mixtures, this competition also determines the autoignition delay time and the associated lift-off height.

In addition to fuel autoignition in vitiated coflow [3], fuel autoignition in preheated coflow air [4,5] represents a useful canonical problem for autoignition that is relevant to practical problems. This configuration has been the subject of a number of experimental and numerical studies, including the more recent work of Echekki and Gupta [6,7], with a limited range of fuels, including hydrogen and syngas. A number of control parameters are found to play an important role in the autoignition process, including the fuel composition, the preheat temperature of the oxidizer, and the inlet conditions (mean flow and turbulence). Flow inlet conditions are associated with the role of the evolving scalar dissipation rate field on autoignition delay. For example, Markides and Mastorakos [4] find that turbulence serves to delay the autoignition process for hydrogen fuels. Similar trends

are found in other studies as well, including a more recent study by Echekki and Gupta [6].

The roles of turbulence and the evolving scalar dissipation field reflect a relatively complex picture of the competition between transport (molecular and turbulent) and chemistry. An earlier study by Mastorakos et al. [8] has shown that autoignition in non-homogeneous mixtures is initiated at variable mixture conditions (composition and temperature) and low rates of dissipation. This observation was further corroborated by subsequent studies with complex chemistry, including the more recent work by Im and Chen [9], Hilbert and Thévenin [10] and Echekki and Chen [11]. Turbulent transport, in addition to the presence of the shear layer separating the fuel and the co-flow, result in the presence of scalar dissipation, which depletes radicals and heat from nascent ignition kernels [11]. Turbulence can serve to modulate the scalar dissipation by either increasing the rate of scalar dissipation or reducing it, as the fuel and oxidizer streams mix.

In this paper, we investigate numerically turbulent jet autoignition using a reduced mechanism for n-heptane using the one-dimensional turbulence (ODT) model [12]. The ODT approach, which is based on 1D unsteady simulations with a stochastic implementation for turbulent transport and a deterministic implementation for the coupling of chemistry and molecular transport, has already been implemented for the study of jet autoignition in hydrogen and hydrogen/carbon monoxide fuels [6,7].

The model represents a valid formulation for jet flames stabilized by autoignition where an inherently parabolic formulation can be adopted. The formulation assumes that downstream effects, especially those responsible for upstream propagation and flame

* Corresponding author.

E-mail address: techekk@ncsu.edu (T. Echekki).

stabilization, do not influence the onset of autoignition or the stabilization mechanism for the jet diffusion flames. It is expected to be valid for a class of lifted flames where the dominant stabilization mechanism is based on autoignition. The study highlights the key roles of molecular and turbulent transport in large hydrocarbon autoignition in a turbulent jet configuration.

N-heptane is an important primary reference fuel for gasoline and diesel fuels. An important feature of n-heptane ignition is the presence of the so-called negative temperature coefficient (NTC). The NTC behavior under certain conditions also results in 2-stage ignition where the temperature initially rises, then, the mixture undergoes a phase of endothermic reactions before the temperature rises again. Within the context of turbulent autoignition, two-stage ignition introduces additional time scales where turbulent and molecular transports can play a role in delaying or enhancing the autoignition process.

2. Model formulations and run conditions

Two sets of simulations are carried out using the 58-species reduced mechanism for n-heptane by Yoo et al. [13]. The mechanism was developed with a two-stage directed relation graph (DRG) approach starting from the LLNL detailed mechanism for n-heptane with 561 species and 2539 reactions [14]. The mechanism was validated using different combustion applications, including ignition, extinction, premixed flame structure and propagation.

The two sets of simulations include:

1. Zero-dimensional homogeneous reaction solver, and
2. One-dimensional stochastic model that emulates combustion in a jet configuration.

The two models are described below.

2.1. Zero-dimensional models

The zero-dimensional simulations for homogeneous ignition are used partly (1) to characterize the autoignition process of n-heptane fuel as a function of mixture fraction given prescribed oxidizer preheat and pre-vaporized fuel temperatures, (2) to identify the most favorable mixture conditions for autoignition and (3) to provide a reference case for comparison with jet autoignition under molecular and turbulent transports.

The governing equations for a zero-dimensional constant pressure system comprised of N chemical species correspond to the species and the temperature equations:

- The species equation:

$$\frac{\partial Y_k}{\partial t} = \frac{\dot{\omega}_k}{\rho}, \quad (1)$$

- The temperature equation:

$$\frac{\partial T}{\partial t} = -\frac{1}{\rho \bar{c}_p} \sum_{k=1}^N h_k \dot{\omega}_k \quad (2)$$

In the above equations, all the symbols have their usual meaning. t is the independent variable, which corresponds to time; T is the temperature; Y_k is the k th species mass fraction; ρ is the mixture density; $\dot{\omega}_k$ is the k th species reaction rates (in dimensions of mass per unit volume per unit time); \bar{c}_p is the mixture specific heat; and h_k is the k th species total enthalpy (combining both chemical and sensible enthalpies). The thermodynamic pressure, p , is assumed to be constant, and the equation of state:

$$\rho = \frac{p}{R_u T \sum_{k=1}^N (Y_k / W_k)}, \quad (3)$$

can be used to determine the mixture density. The governing equations are integrated using a modified version of the CHEMKIN II code

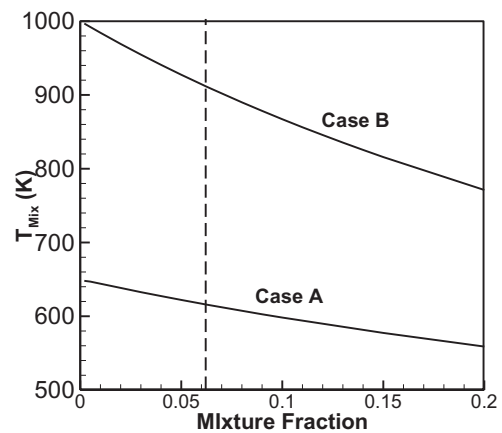


Fig. 1. Initial mixture temperature based on the prescribed mixture fraction for cases A and B. The stoichiometric condition is shown with the dashed line.

SENKIN [15]. The system is integrated using a variant of the DASSL software called DASAC [16].

The simulations are designed to complement the jet studies, which prescribe unique temperatures for the oxidizer and the fuel. A range of mixture fractions are considered where the fuel and oxidizer are mixed adiabatically at fixed pressure (i.e. constant enthalpy) to yield a mixture composition and temperature. Given that the oxidizer is preheated, the fuel-lean conditions (i.e. low mixture fractions) have higher temperatures than the fuel-rich conditions.

In these studies we have prescribed the fuel and oxidizer temperatures, T_{fuel} and T_{oxid} , and varied the mixture composition from fuel-lean to fuel-rich by prescribing a mixture fraction (0 for all oxidizer, 1 for all fuel), Z . The initial mass fraction for a given k th species in the mixture for a given mixture fraction is prescribed based on its composition in the fuel and the oxidizer and the mixture fraction as follows:

$$Y_k = Z \times Y_{k,\text{Fuel}} + (1 - Z) \times Y_{k,\text{Oxidizer}} \quad (4)$$

where the subscripts “Fuel” and “Oxidizer” refer to the mass fractions of the k th species in the fuel and the oxidizer streams, respectively. The mixture temperature, T_{mix} , is prescribed by solving the solutions for adiabatic mixing:

$$\begin{aligned} Z \times h_{\text{Fuel}}(T_{\text{Fuel}}) + (1 - Z) \times h_{\text{Oxidizer}}(T_{\text{Oxidizer}}) \\ = Z \times h_{\text{Fuel}}(T_{\text{mix}}) + (1 - Z) \times h_{\text{Oxidizer}}(T_{\text{mix}}) \end{aligned} \quad (5)$$

The mixture conditions corresponding to this study correspond to a reference state of pre-vaporized fuel at 400 K and 1 atm and two different air preheat temperatures at 650 K, identified as case A, and 1000 K, identified as case B, both at atmospheric pressures.

The run conditions were selected around the stoichiometric mixture fraction of 0.0621 and range for values of the mixture fraction from 0.002 to 0.2. Figure 1 shows the initial mixture temperatures for both cases A and B based on the values of the mixture fractions considered. Because of the differences between the specific heats of the fuel and the oxidizer species, the initial mixture temperature profiles are not linear in mixture fraction space.

2.2. One-dimensional turbulence (ODT) model

Practical configurations of combustion of n-heptane fuel invariably require combustion in a turbulent environment. We are using a very powerful and relatively low-computational cost tool to advance our understanding of autoignition in turbulent media. The tool is based on simulations using the stand-alone one-dimensional turbulence (ODT) approach. A detailed description of the ODT model formulation for the jet configuration is given by Echehki et al. [12].

The model was implemented as a stand-alone model for the study of other jet diffusion flames as well [17–21]. The ODT model is based on a deterministic implementation of reaction and diffusion and a stochastic implementation of turbulent advection in a space- and time-resolved simulation on a 1D domain. In this problem, the 1D domain corresponds to the transverse direction of the mean flow. The temporal evolution of the 1D profile for the streamwise momentum, energy and the species equations is interpreted as a downstream evolution of the jet transverse profiles. The molecular processes are prescribed by the following unsteady reaction–diffusion equations:

- The streamwise momentum equation:

$$\frac{\partial u}{\partial t} = \frac{1}{\rho} \frac{\partial}{\partial y} \left(\mu \frac{\partial u}{\partial y} \right), \quad (6)$$

- The species equation:

$$\frac{\partial Y_k}{\partial t} = -\frac{1}{\rho} \frac{\partial}{\partial y} (\rho V_k Y_k) + \frac{\dot{\omega}_k}{\rho}, \quad (7)$$

- The temperature equation:

$$\frac{\partial T}{\partial t} = \frac{1}{\rho \bar{c}_p} \sum_{k=1}^N c_{p,k} Y_k V_k \frac{\partial T}{\partial y} + \frac{1}{\rho \bar{c}_p} \frac{\partial}{\partial y} \left(\lambda \frac{\partial T}{\partial y} \right) - \frac{1}{\rho \bar{c}_p} \sum_{k=1}^N h_k \dot{\omega}_k \quad (8)$$

In the above equations, all the symbols have their usual meaning. The thermodynamic pressure, p , is assumed to be spatially uniform, and the equation of state (Eq. (3)) is used again to determine the mixture mass density, ρ . $c_{p,k}$ and V_k represent the k th species specific heat and diffusion velocity, respectively and λ is the mixture thermal conductivity.

Eqs. (6)–(8) represent a temporal solution of a turbulent jet flame. The temporal evolution of the solution represents a downstream evolution of the spatial profiles of the solution vector. The temporal evolution is interpreted as a downstream spatial evolution (in x) of the 1D velocity and scalar profiles using the following equations [12]:

$$\bar{u} - u_\infty = \frac{\int_{-\infty}^{+\infty} \rho(u - u_\infty)^2 dy}{\int_{-\infty}^{+\infty} \rho(u - u_\infty) dy} \quad \text{and} \quad x(t) = \int_0^t \bar{u}(t') dt' \quad (9)$$

where \bar{u} and u_∞ correspond, respectively, to a bulk velocity and the co-flow velocity.

Turbulent advection is implemented stochastically using stirring events, each involving the application of a ‘triplet map’ [12]. The frequency of stirring events is governed by the spatially-resolved evolving rate of shear in the jet. The stirring events are implemented as a parallel process to the deterministic solution for the streamwise velocity, species mass fractions and temperature. A stirring event involves the random selection of a size \hat{l} and position \hat{y} of an eddy based on prescribed distributions (uniform for position and a distribution proportional to \hat{l}^{-2} for the size). However, the algorithm eventually reconstructs the distribution of the positions and sizes of the eddies based on the rate of shear in the jet. Further discussion of the implementation of turbulent advection is provided in Ref. [12]. Two adjustable parameters, the so-called A and β [12], are identical to previous values used in jet configurations with ODT well [17–21]. The parameter A is of order unity and relates the local shear experienced by the eddy to its characteristic time τ . The parameter β also is of order unity. It relates an eddy turnover time to the time elapsed during the simulations and is used to inhibit large eddies from occurring towards the inlet of the jet, such that stirring events are allowed only when $t \geq \beta \tau$.

The temporal discretization of the governing equations is based on full splitting of diffusion and reaction in which diffusion is advanced using the first-order Euler method, while the source term is integrated using a stiff-integrator, DVODE [22]. A second-order finite-difference scheme is used for spatial discretization. Transport

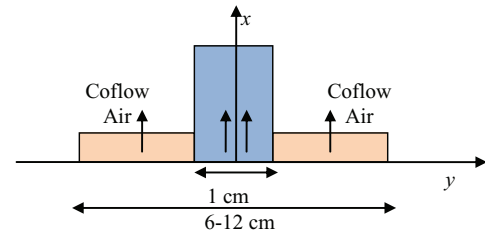


Fig. 2. Computational configuration and initial run condition. The relative sizes of the boxes indicate that the fuel jet exit velocity is higher than the co-flow velocity.

properties for heat and mass are based on a mixture-averaged formulation and computed using transport libraries [23] within the Chemkin II suite [24]. The boundaries of the ODT computational domain are maintained at free-stream conditions throughout the jet. In the present implementation, dilatation is accompanied by an expansion of the computational cells on the 1D domain proportional to the density decrease [25]. The computer code is written in Fortran and is implemented as an application coupled with Chemkin II libraries.

Figure 2 shows the computational setup for the jet simulations. The initial configuration consists of a 2D segregated fuel jet with heated air in the co-flow. The fuel jet has a fixed width of 1 cm; while, the extent of the co-flow jet is prescribed based on the growth of the boundary layer throughout the simulation, such that higher jet inlet velocities required a higher range for the co-flow length. The fuel and preheated co-flow air are prescribed with their temperatures and inlet velocity. In all cases, considered, the fuel is considered as pre-vaporized fuel with an inlet temperature of 400 K and 1 atm. The oxidizer preheat has a temperature of either 650 K (case A from the homogeneous mixture studies) or 1000 K (case B from the homogeneous mixture studies). The co-flow velocity is fixed at 1 m/s; while, different fuel jet inlet Reynolds numbers are considered including 5000, 10,000, 20,000, 40,000 and 60,000.

3. Results: homogeneous ignition

In this section, we present results of the homogeneous ignition studies. An important element of the discussion is the ignition delay time and whether there is a presence of two-stage ignition vs. single-stage ignition. We are using two methods to evaluate the time for the onset of any ignition stage, which correspond to the presence of a local peak of the temperature gradient and a local peak of the OH mass fraction. The temporal evolution of temperature and OH and HO₂ mass fractions are shown first to demonstrate the temporal evolution of these quantities.

Figure 3 shows the temporal evolution of the temperature for 4 different mixture conditions, $Z = 0.005, 0.02, 0.1$ and 0.15 for case A. Although not clear for mixture fractions 0.1, the three mixture fractions, 0.005, 0.02 and 0.1, exhibit a two-stage ignition process characterized by an initial rise of the temperature, indicating a rapid heat release, followed by a second rise. The gap between the two stages decreases as the mixture fraction increases. They are fully merged at $Z = 0.15$. Both $Z = 0.1$ and 0.15 also show an overshoot of the temperature at the end of the second ignition stage. Out of the 4 mixture fractions shown, $Z = 0.02$ exhibits the lowest ignition delay time for both stages.

Figure 4 shows similar profiles to Fig. 3 corresponding to case B where the oxidizer preheat temperature is higher at 1000 K. Mixture fractions 0.05, 0.02 and 0.1 now exhibit only a single ignition stage. While $Z = 0.15$ still exhibits a two-stage ignition process. Therefore, in contrast with case A, case B exhibits two-stage ignition at richer mixtures. Moreover, the latter two mixture fractions, $Z = 0.1$ and 0.15 , exhibit a temperature overshoot before the termination stages of the autoignition process. Also, similarly to case A, mixture fraction $Z = 0.02$ exhibits the lowest ignition delay time for both stages.

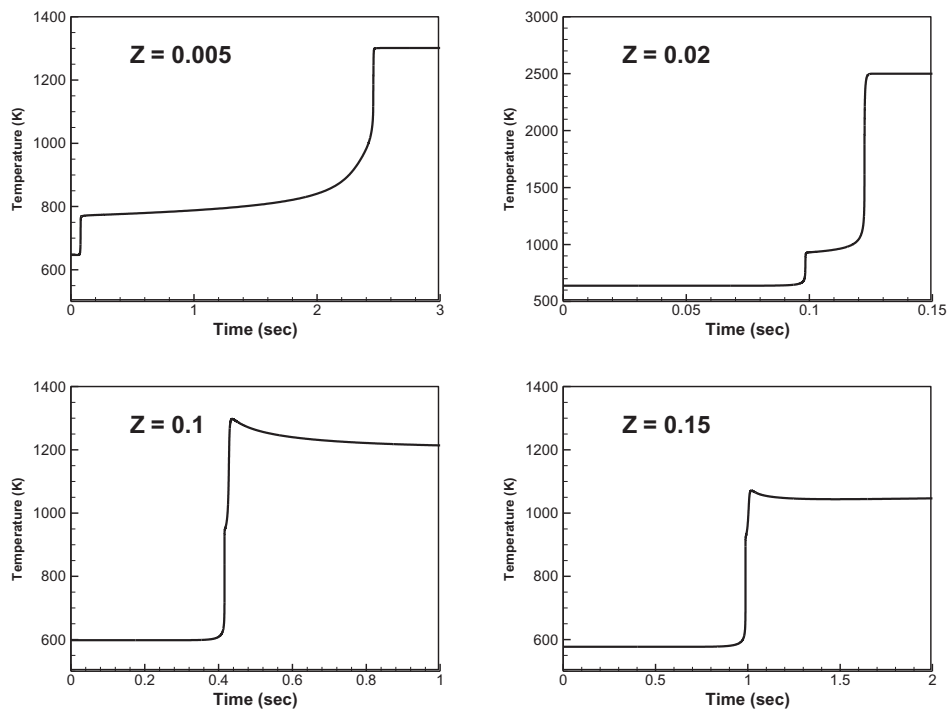


Fig. 3. Evolution of temperature during ignition for Case A at different mixture fractions.

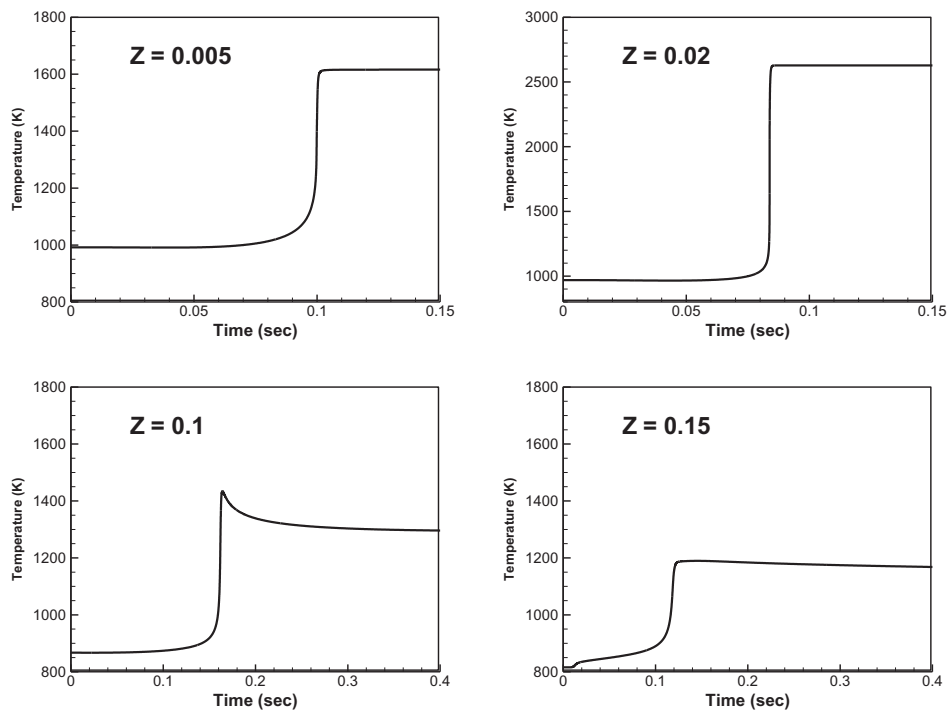


Fig. 4. Evolution of temperature during ignition Case B at different mixture fractions.

Also, for both cases, this mixture fraction exhibits the highest temperature rise given the fact that mixture fractions are much different from the stoichiometric value result in excess fuel or excess oxidizer that tends to lower the adiabatic flame temperature. However, in contrast to case A, there is no significant variation in the ignition delay times for the different mixture fractions shown. This difference may play an important role in reducing transport effects on ignition delay time in the presence of scalar dissipation.

The weak dependence of the ignition delay time on mixture fraction in case B has been observed in a number of studies, including the recent work by Zhao and Law [26]. In that study, Zhao and Law [26] have observed that the total ignition delay time for n-heptane-air mixtures at 1 atm and different equivalence ratios (from lean to rich) are comparable at a temperature just below 1100 K and little variability at temperatures corresponding to the range of temperatures illustrated in Fig. 7.

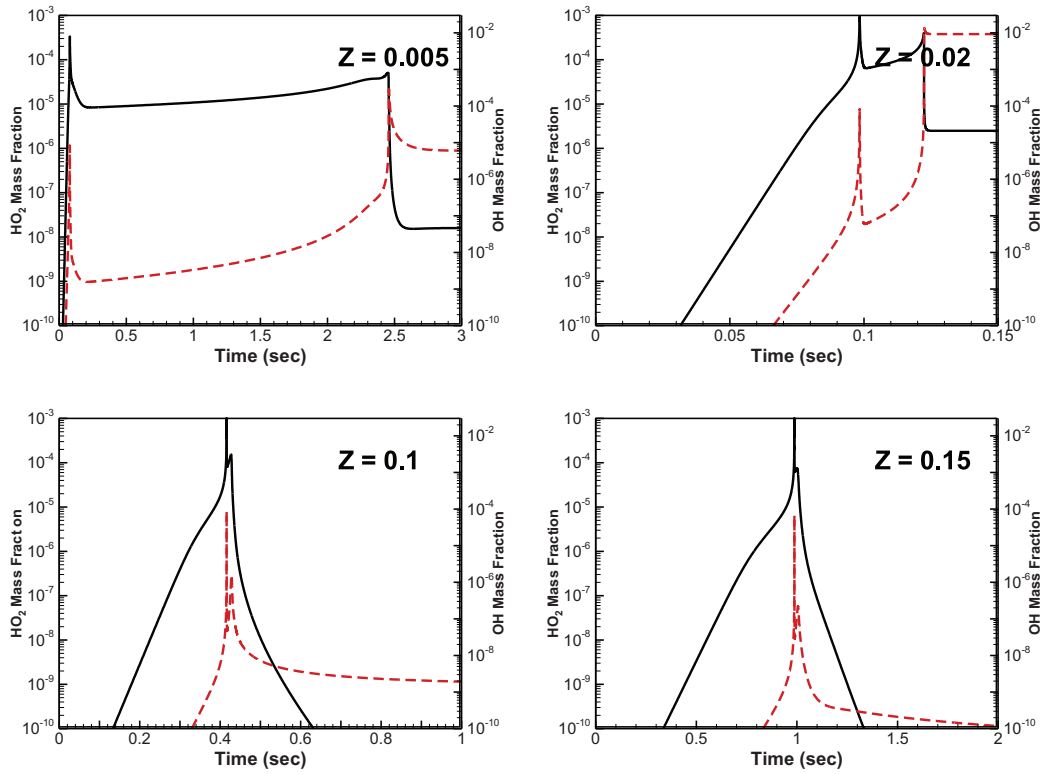


Fig. 5. Evolution of HO₂ (solid-black) and OH (dashed-red) mass fractions for case A at different mixture fractions. (For interpretation of the references to color in this figure legend, the reader is referred to the web version of this article).

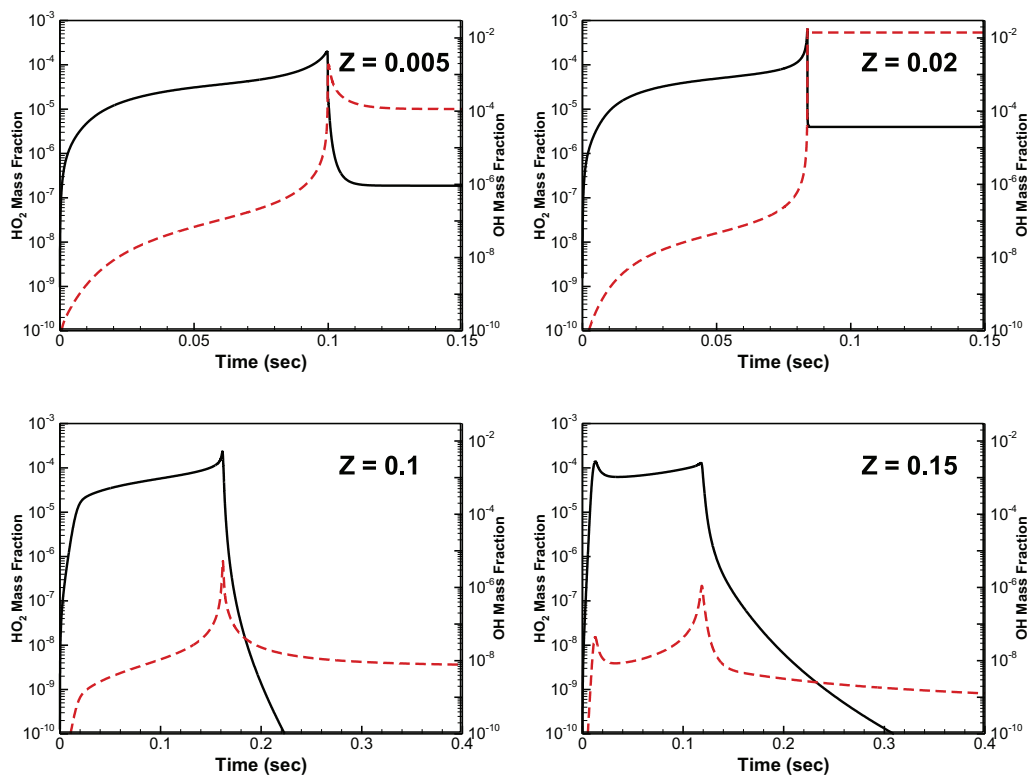


Fig. 6. Evolution of HO₂ (solid-black) and OH (dashed-red) mass fractions for case B at different mixture fractions. (For interpretation of the references to color in this figure legend, the reader is referred to the web version of this article).

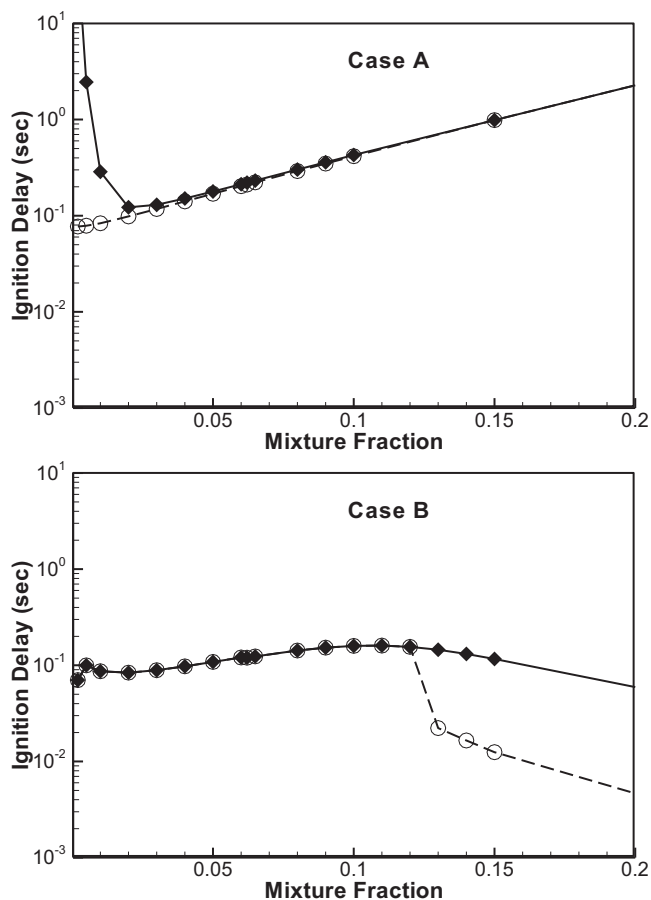


Fig. 7. Variation of the first (dashed) and second (solid) stage ignition delay times with mixture fraction.

Figure 5 shows the HO_2 and OH mass fraction temporal profiles corresponding to case A and the mixture fractions illustrated in Fig. 3. The figure shows a prominent role played by HO_2 during the induction stages (prior to each temperature rise). The profiles also are closely correlated with those of OH, which only become larger once the final stage of ignition is completed. The positions of the OH peaks and those of temperature peak gradients with respect to other time scales (e.g. ignition delays or times between stages) are reasonably close to rely primarily on one to determine the ignition delay.

Figure 6 shows the HO_2 and OH temporal profiles corresponding to case B and the mixture fractions illustrated in Fig. 4. Here, mixture fraction $Z = 0.15$ clearly exhibits the two-stage ignition process with two peaks for HO_2 and OH. Similar observations regarding the choice of ignition criteria can be made here for OH and temperature gradients.

Figure 7 presents the ignition delay times corresponding to the first (dashed) and second (solid) stages of the ignition as functions of the mixture fraction for the ranges of mixture fractions considered for both cases A and B. The figure confirms some of the key observations made from Figs. 3–6:

- The two-ignition process is found at the lowest values of the mixture fractions for case A for the range of mixture fractions considered where the gap between the two stages is also highest. The opposite trend is observed for case B where the gap between the two stages is higher at higher mixture fractions.
- The ignition delay times corresponding to case B are lower owing to their higher oxidizer preheat temperatures. The trend is sustained for a wider range of the mixture fractions where variations in second ignition delay are within a factor of 2–3 times.

Meanwhile, there is a large variation in the values of the ignition delay times for case A.

- The final ignition stage (solid lines in Fig. 7) exhibits a local minimum for case A at values of the mixture below the stoichiometric value. This condition balances two competing effects, which corresponds to higher temperatures towards leaner mixture conditions and the excess oxidizer in these mixtures. In contrast, several minima are exhibited for case B, which correspond to both effects of preheat and the ability of the first ignition stage to generate important radicals that will precipitate the second ignition stage. This trend is shown in Fig. 6, which illustrates higher concentrations of HO_2 and OH for $Z = 0.15$ compared to $Z = 0.1$.

4. Results: turbulent jet autoignition

In this section, the process of autoignition in turbulent jet diffusion flames is investigated. As stated earlier, two mixture conditions are considered corresponding to different preheat temperatures. For these two conditions, the (fuel) jet inlet Reynolds numbers are varied from 5000 to 60,000. The autoignition process is discussed using instantaneous spatial profiles at different times for representative thermo-chemical scalars. Statistics conditioned on the mixture fraction also are used. The discussion builds on our observations based on homogeneous ignition.

Figures 8–11 show spatial profiles of temperature and HO_2 mass fraction for case A at different times $t = 0.06, 0.12, 0.18$ and 0.24 s and for the jet Reynolds numbers of 5000, 10,000, 2000 and 40,000, respectively. The time 0.12 s corresponds approximately to the time of the earliest ignition in the homogeneous mixture corresponding to a mixture fraction near 0.02. We have chosen to plot additional results at increments of 0.06 (one below 0.12 and 2 above 0.12). Increasing the jet inlet Reynolds number from 5000 to 40,000 also increases turbulence effects.

As Fig. 8 shows, there are two peaks of HO_2 mass fraction at 0.06 s. These peaks correspond to the presence of two mixing layers at the interface of the fuel and the oxidizer. Under laminar conditions, autoignition would start at these layers and would exhibit two identical peaks around the position 0. At 0.06 s no stirring events have occurred yet. However, even if turbulence effects are not present at this time, molecular diffusion effects are. The presence of additional fluctuations at later times indicates the presence of turbulent stirring events whose sizes correspond to the contribution of various eddies in the 3D context.

As the temperature profiles in Fig. 8, the presence of temperature peaks at 0.18 s indicates an autoignition process that has already started and the formation of two autoignition kernels, with one (on the right) exhibiting a higher temperature than the second one (on the left). This difference can be attributed to the presence of stirring events at an earlier stage (see the figure at 0.12 s), which increases the local dissipation rate and contributes to a reduction in the radical species (e.g. HO_2) in the nascent kernel. However, a higher temperature is seen on the left kernel at 0.24 s. Different mechanisms can contribute to the reversal of trends in this case and others. One possible mechanism is that a higher rate of dissipation precipitates its evolution to a lower value and a reduction in heat and radical losses at nascent kernels. A second mechanism may be attributed to an onset of autoignition at mixture conditions that would yield a higher adiabatic temperature.

Figures 9–11 illustrate some of the effects of turbulence on the autoignition process. Increasing scalar fluctuations with higher Reynolds numbers for the same times indicates a higher rate of stirring events, which tend to “break up” nascent kernels. No new peaks of temperature can be seen at times 0.06, 0.12 and 0.18 s indicating further ignition delay due to turbulence. The profiles at 0.24 s show that autoignition has already started. They also show that, with increasing stirring events, the mixture is made more homogeneous

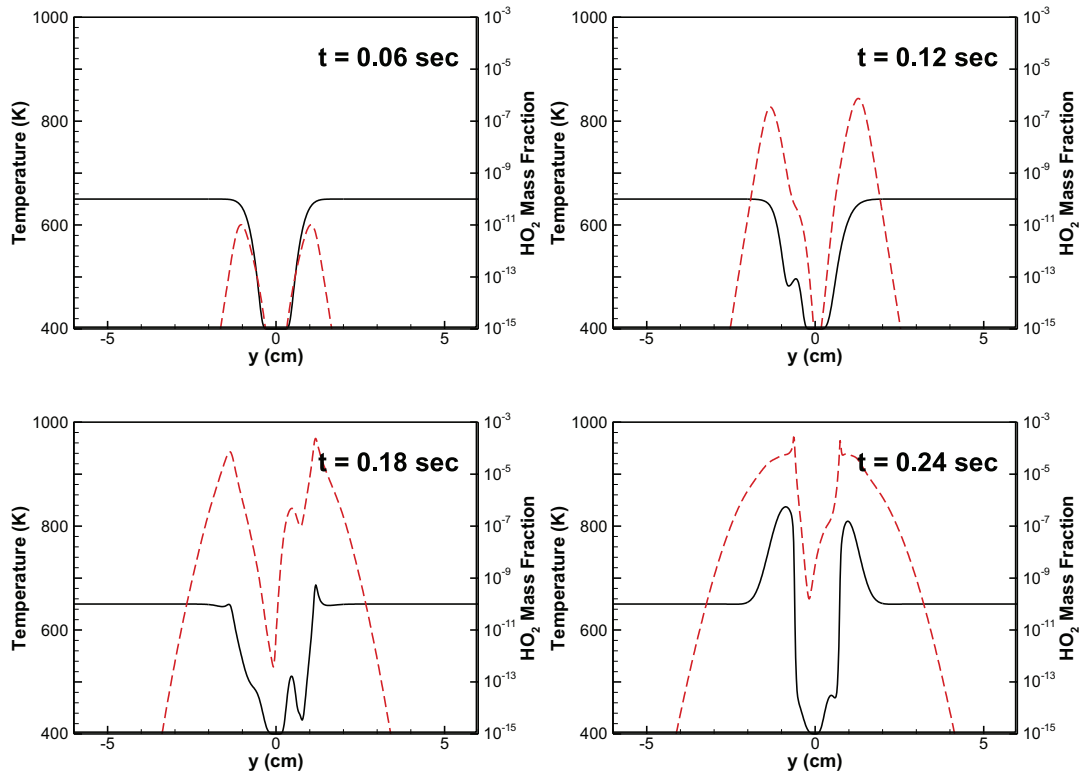


Fig. 8. Temperature (solid) and HO₂ (dashed) profiles at different times of the jet evolution for Case A and Re = 5000.

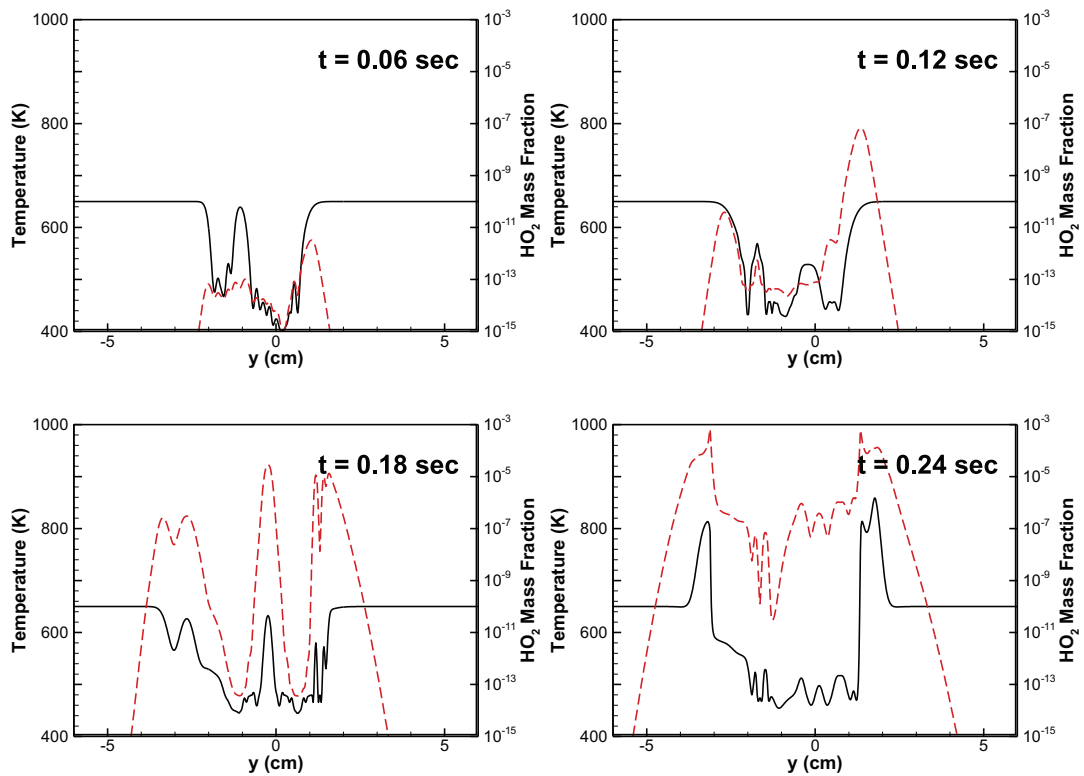


Fig. 9. Temperature (solid) and HO₂ (dashed) profiles at different times of the jet evolution for Case A and Re = 10,000.

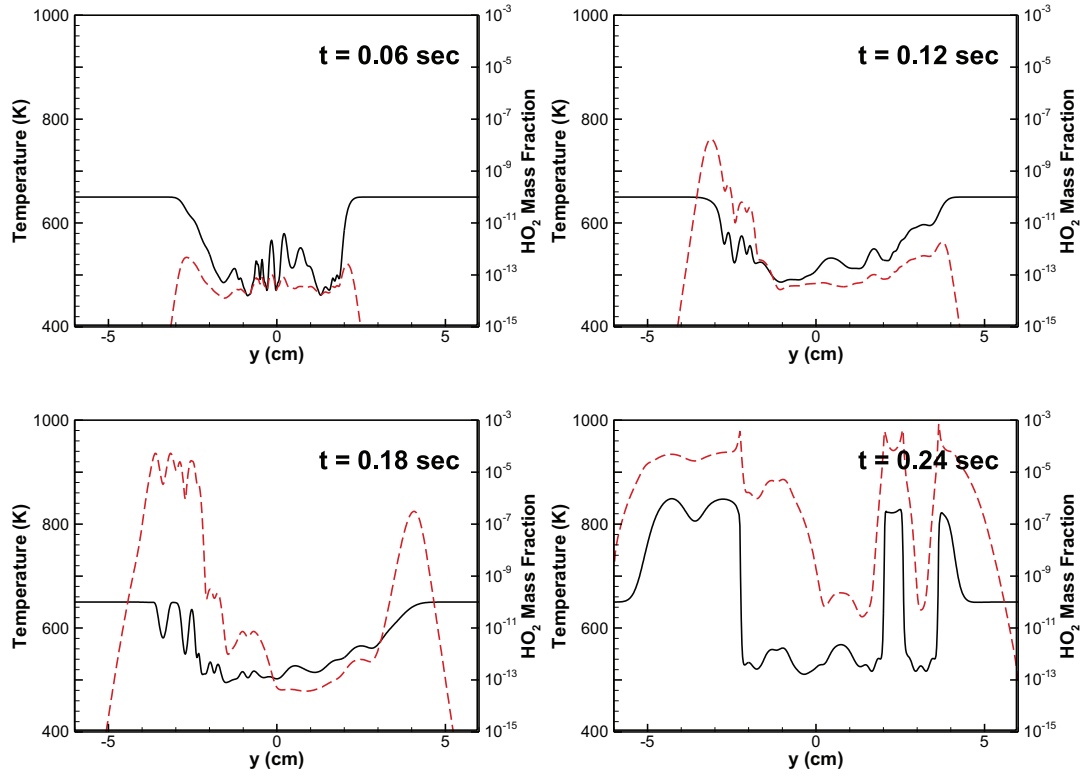


Fig. 10. Temperature (solid) and HO₂ (dashed) profiles at different times of the jet evolution for Case A and Re = 20,000.

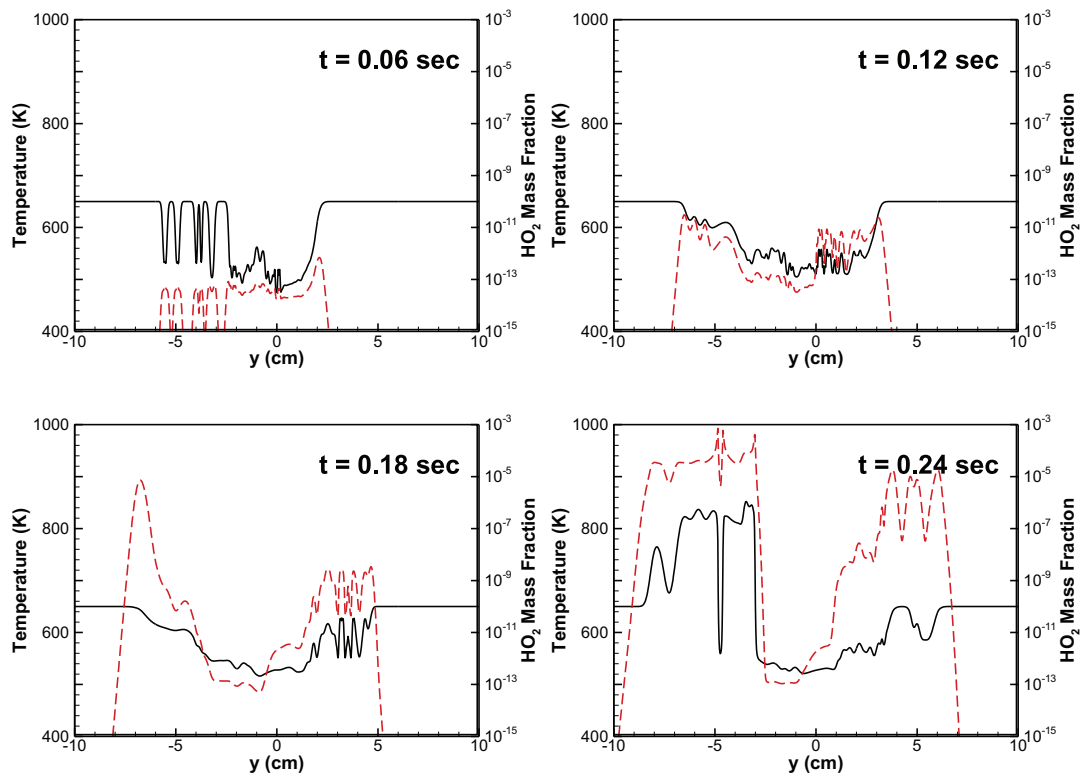


Fig. 11. Temperature (solid) and HO₂ (dashed) profiles at different times of the jet evolution for Case A and Re = 40,000.

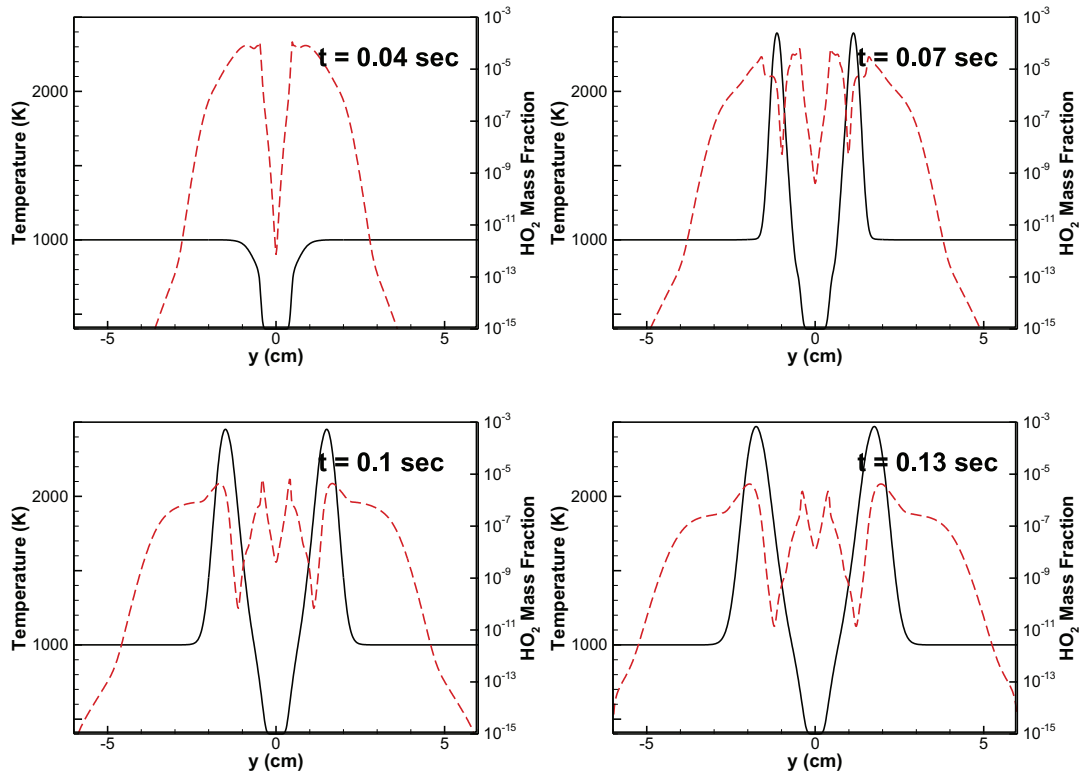


Fig. 12. Temperature (solid) and HO₂ (dashed) profiles at different times of the jet evolution for Case B and Re = 5000.

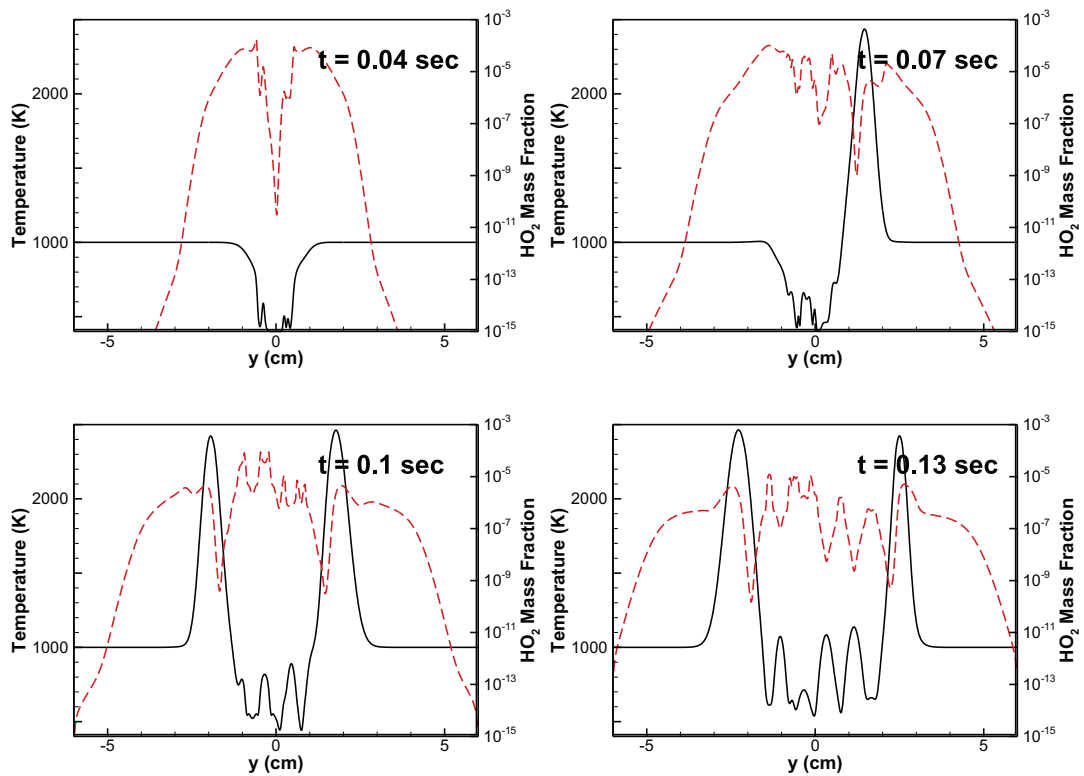


Fig. 13. Temperature (solid) and HO₂ (dashed) profiles at different times of the jet evolution for Case B and Re = 10,000.

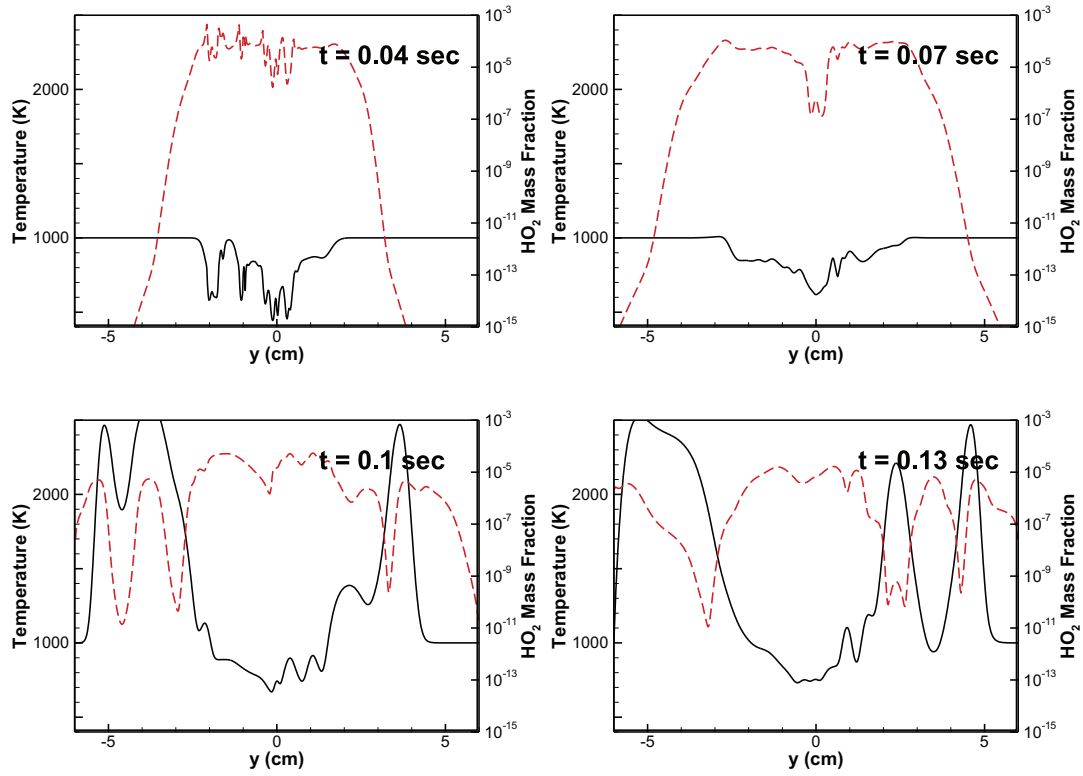


Fig. 14. Temperature (solid) and HO₂ (dashed) profiles at different times of the jet evolution for Case B and Re = 20,000.

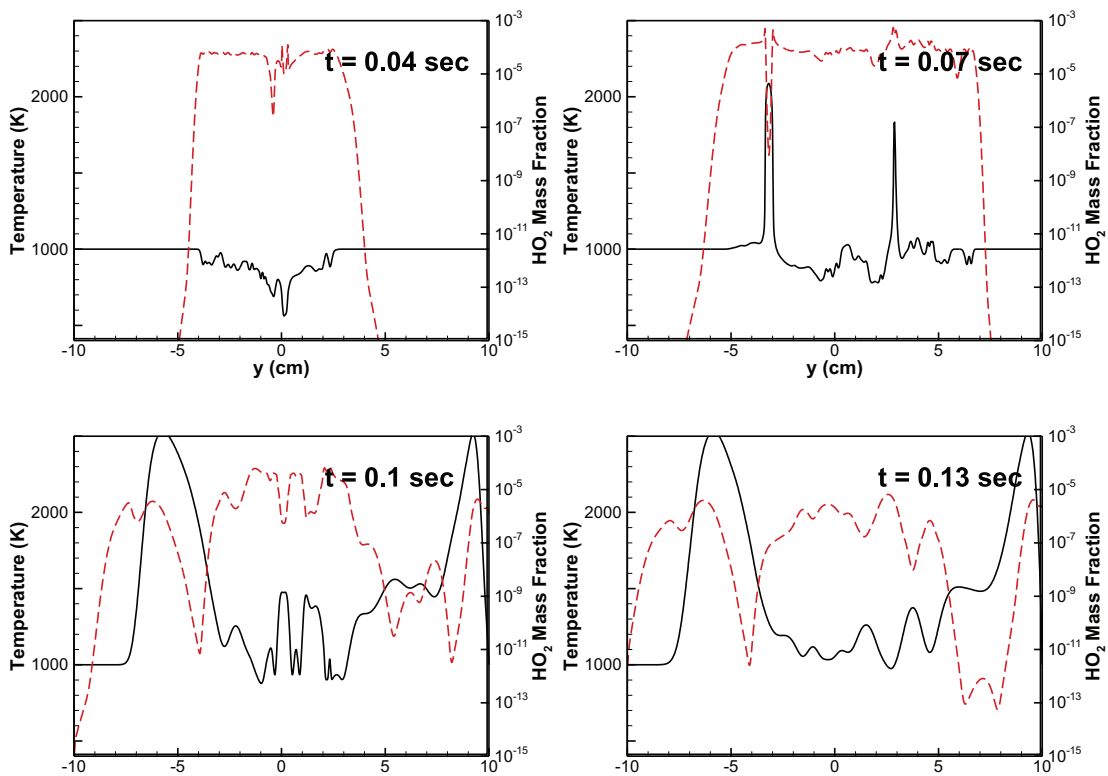


Fig. 15. Temperature (solid) and HO₂ (dashed) profiles at different times of the jet evolution for Case B and Re = 40,000.

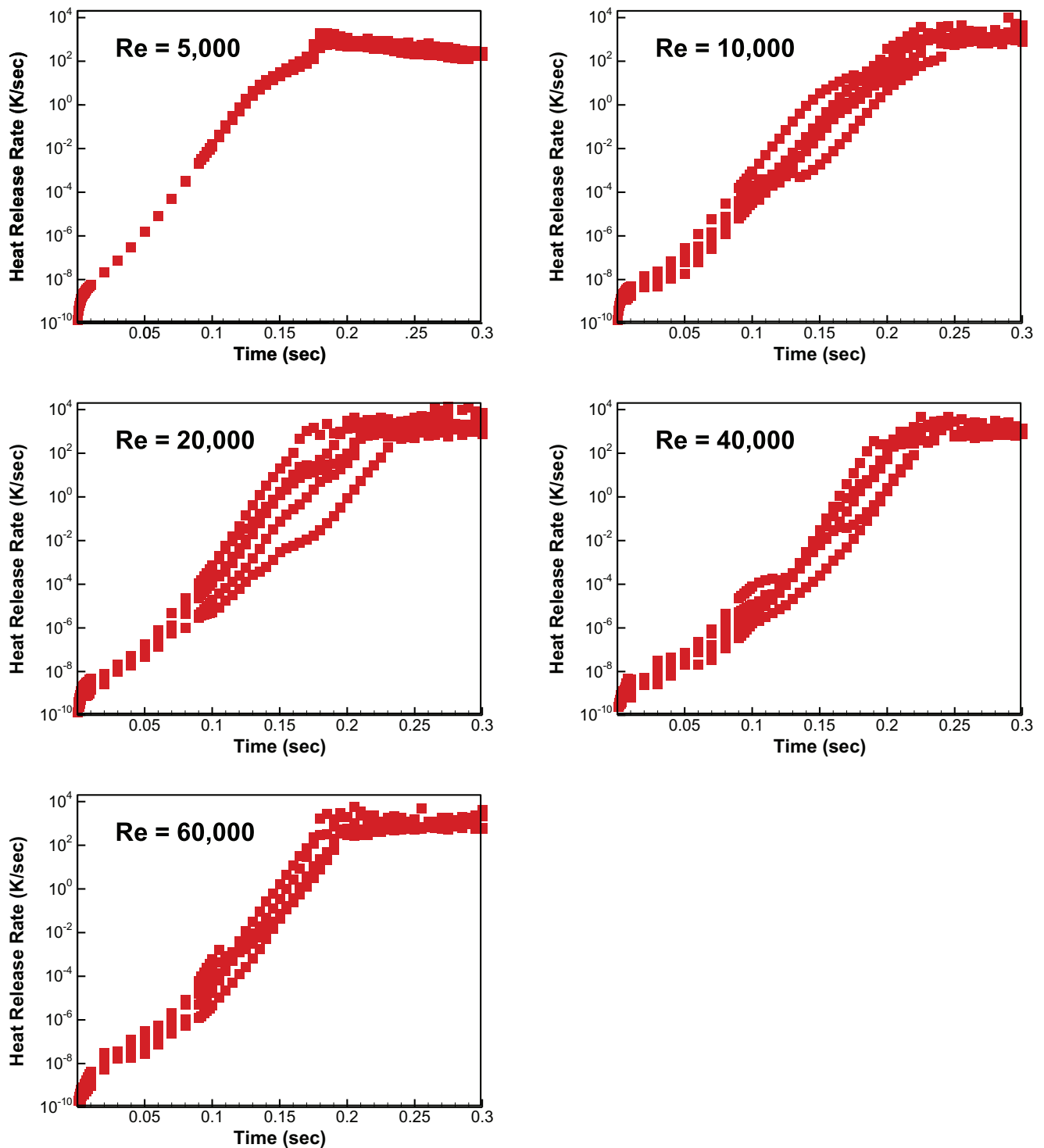


Fig. 16. Temporal evolution of the integrated heat release rate for $Re = 5000, 10,000, 20,000, 40,000$ and $60,000$ for case A.

quickly at various patches of the mixture. Nascent kernels merge to generate potentially larger kernels. The high temperature peaks at higher Reynolds numbers also are broader, also suggesting a higher rate of post-ignition, high-temperature combustion.

Figures 12–15 show spatial profiles of temperature and HO_2 mass fractions similar to Figs. 8–11, but for case B, and showing results for times $t = 0.04, 0.07, 0.13$ and 0.16 s. In Fig. 6, some of the earliest autoignition delay times indicated correspond to approximately to 0.08 s at $Z = 0.02$.

Figure 12 shows the presence of two ignition kernels at a much earlier time than the earliest ignition delay times for the homogeneous mixture. As the temperature profiles show, no stirring events are present at $t = 0.04$ s. Therefore, the mechanism that precipitates ignition may be attributed to molecular transport, which is not present in the homogeneous ignition scenarios.

The role of molecular transport in precipitating autoignition has been identified in earlier studies (see for example, [6,27–29]). For example, Echekki and Gupta [6] have identified the role of the

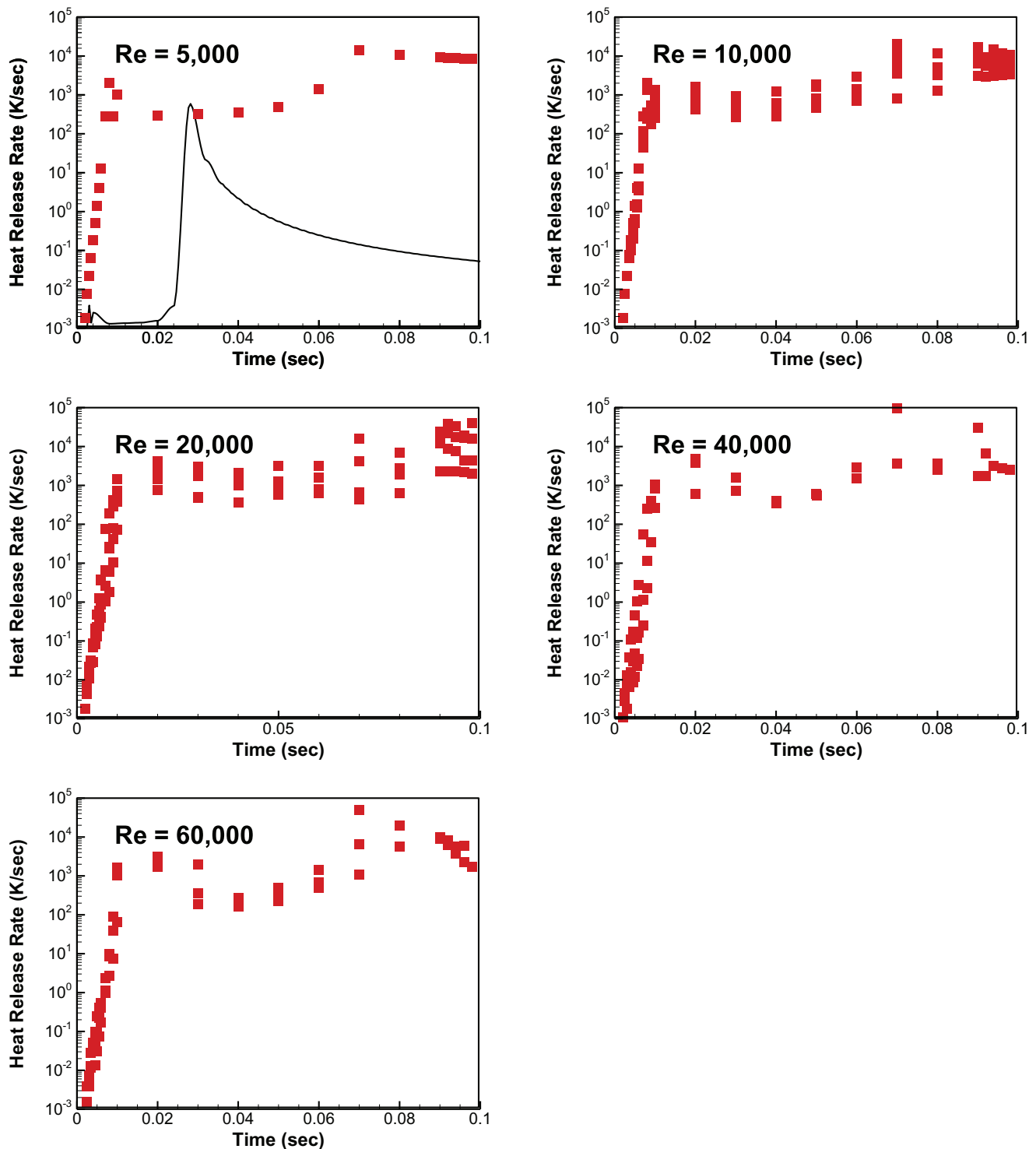


Fig. 17. Temporal evolution of the integrated heat release rate for $Re = 5000, 10,000, 20,000, 40,000$ and $60,000$ for case B.

differential diffusion of H_2 relative to CO in a CO/H_2 -air jet similar to the one adopted here as the mechanism for precipitating autoignition relative to homogeneous mixtures. In fact, at the onset of autoignition, the H_2/CO ratio is higher than the corresponding value in the pure fuel stream.

Van Oijen [27] also investigated the autoignition process of H_2/CH_4 -air in a mixing layers using direct numerical simulations. Van Oijen has found that the preferential diffusion of H_2 into the pre-heated air stream also does contribute the precipitating the autoignition process relative to homogeneous reactor simulations.

Finally, temperature stratifications in the co-flow are also found to play a role in precipitating autoignition with increased turbulence as demonstrated by the lower lift-off heights/ignition delay times, respectively, in both experiments [28] and computations [29], respectively, for co-flowing streams of natural gas with hot vitiated air. In both studies, [28] and [29], turbulence is able to bring a hotter co-flow into the ignition zone.

In our study, involving a single-component fuel, n-heptane, we believe that the mechanism that results in earlier ignition may be attributed to the onset of first-stage ignition in nearby richer mixture

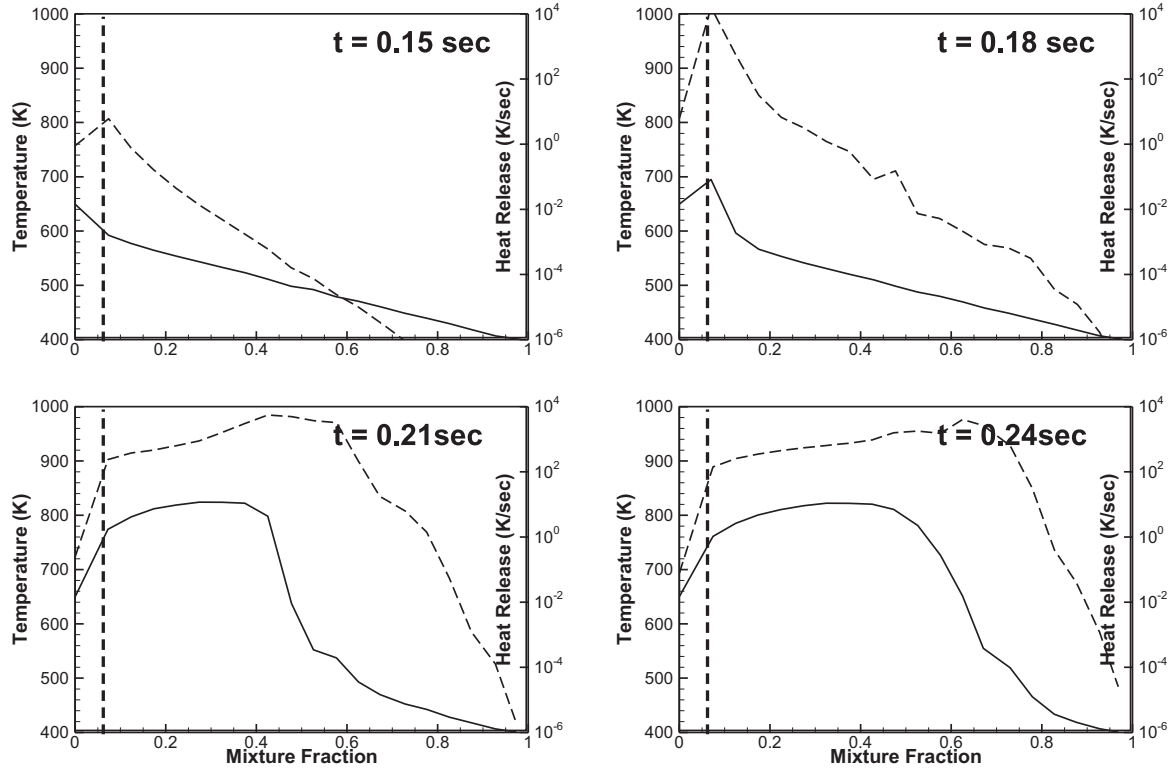


Fig. 18. Conditional means of temperature (solid) and heat release rate (dashed) for $Re = 5000$ and case A. The vertical dashed line corresponds to a stoichiometric mixture.

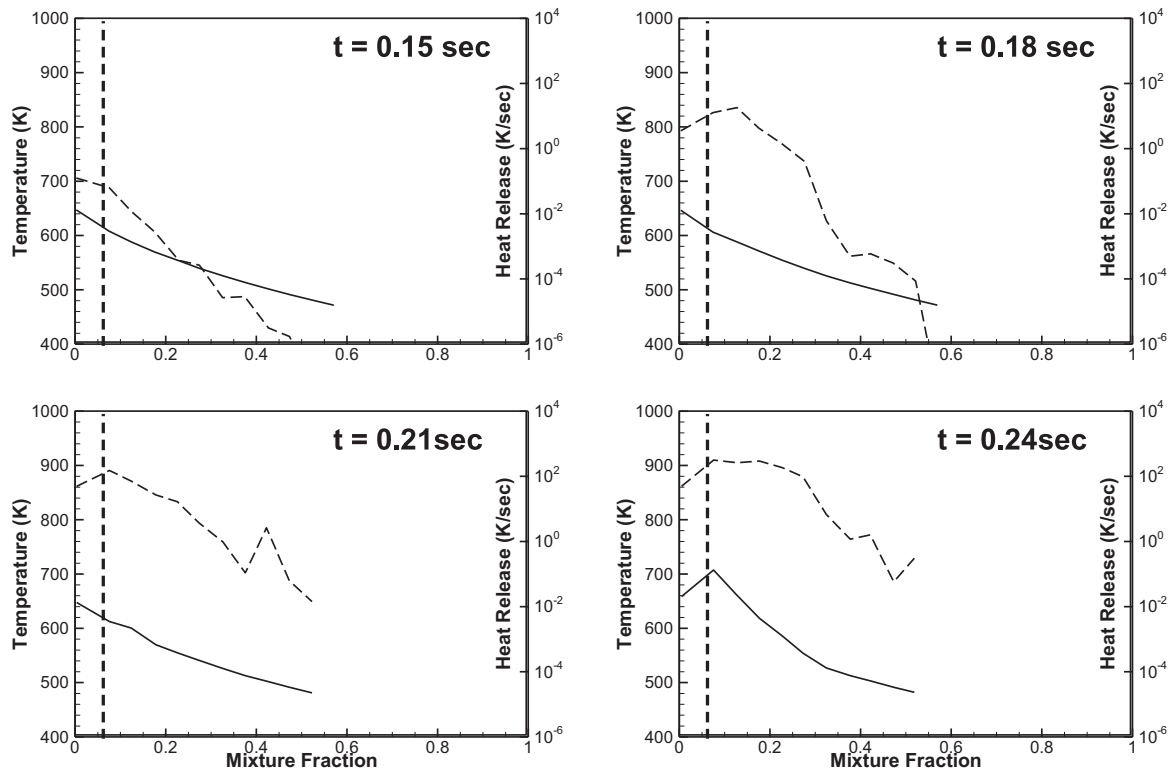


Fig. 19. Conditional means of temperature (solid) and heat release rate (dashed) for $Re = 20,000$ and case A. The vertical dashed line corresponds to a stoichiometric mixture.

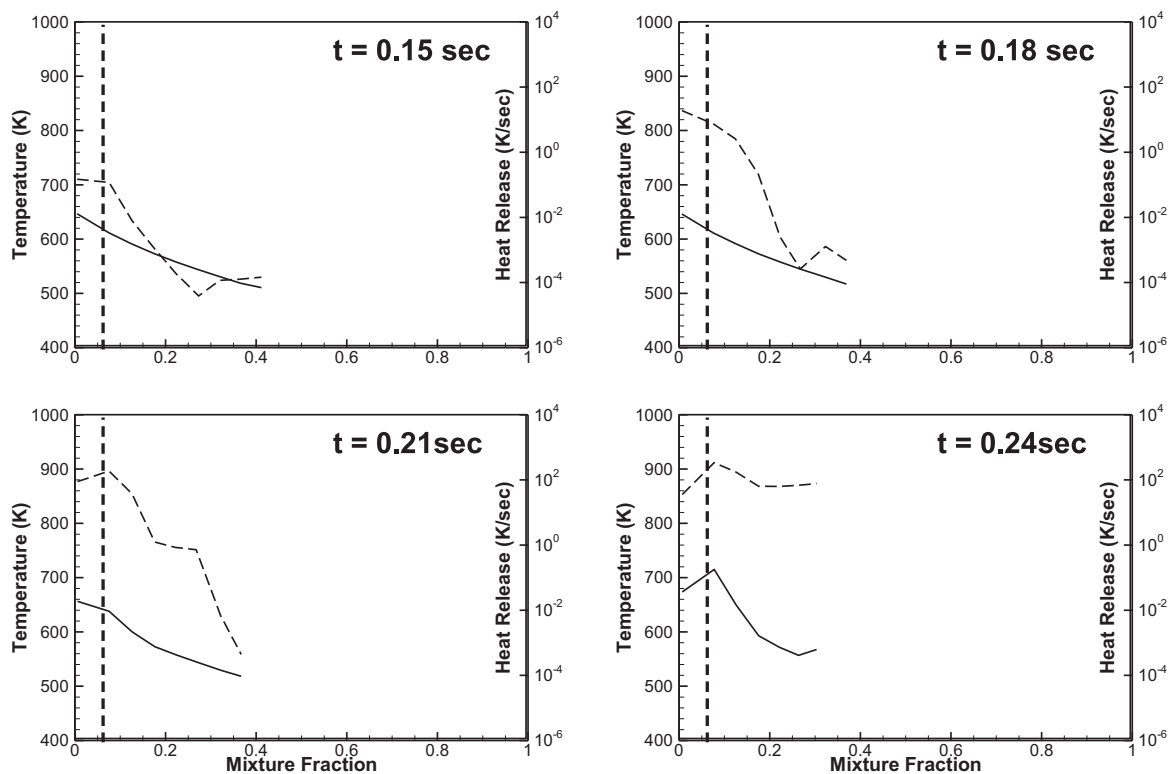


Fig. 20. Conditional means of temperature (solid) and heat release rate (dashed) for $Re = 60,000$ and case A. The vertical dashed line corresponds to a stoichiometric mixture.

as a first step to preheat the most favorable sites for ignition (i.e. at leaner mixture) and precipitate the final ignition stage at these mixtures. Therefore, the mechanism is governed by transport, which is preceded by heat release.

Figures 12–15 clearly show that the presence of turbulence does again result in autoignition delay; but, the trend is non-monotonic. At 0.07 s, there is only one autoignition kernel for $Re = 5000$, no ignition kernels for $Re = 10,000$, and, then, two autoignition kernels for $Re = 40,000$. Again, this non-monotonic behavior as a function of Reynolds numbers reflects the presence of two effects that compete on similar time scales. First, the presence of stirring events, characteristic of turbulence, tends to increase the rate of dissipation and delay the onset of autoignition. However, the same events also tend to homogenize the mixture (as shown through the comparison of the temperature profiles at 0.04 s between $Re = 20,000$ and $Re = 40,000$, resulting in the eventual decay of scalar dissipation. If this occurs early enough, the more homogeneous mixture, which does not exhibit a significant autoignition delay for case B ignites, and may ignite sooner than autoignition kernels delayed by scalar dissipation (as seen in Fig. 13 for $Re = 10,000$). Therefore, the mechanisms governing autoignition or its delay under turbulence conditions and in the jet configuration can be competitive.

Another perspective of the trends observed for cases A and B can be illustrated using the spatially integrated heat release rate profiles corresponding to 20 realizations of the ODT simulations for the different Reynolds numbers, 5000, 10,000, 20,000, 40,000 and 60,000. Figures 16 and 17 show the temporal evolution of the integrated chemical source term for these Reynolds numbers for cases A and B, respectively. The integrated chemical source term is expressed as: $-\int_{y_{\min}}^{y_{\max}} (\frac{1}{\rho c_p} \sum_{k=1}^N h_k \dot{\omega}_k) dy$. This term represents the 1D spatial integrated contribution from chemistry to the right-hand side of the temperature Eq. (8).

From the figures, the following can be observed. First, the integrated heat release profiles for case B exhibit an initial peak at periods between 0.01 and 0.02 s that appears to be primarily associated

with the first stage of autoignition at mixture fractions higher than the stoichiometric values. We have indicated earlier that two-stage ignition for case B occurred at mixture fractions greater than 0.1.

For case A, there is only a single peak. The scatter plot for the heat release rate in this case shows the most spread at intermediate Reynolds number values, especially at $Re = 20,000$, and not necessarily at the highest Reynolds numbers. The case of $Re = 5000$ exhibits a nearly laminar behavior with the least spread. We believe that this trend is attributed to the competition of the time scales associated with ignition chemistry and turbulent time scales. At the lower Re values, chemical time scales are more dominant; while, at much higher time scales, turbulent length scales tend to quickly homogenize the mixture as it evolves from multiple ignition kernels to fewer and merged kernels.

For case B, the higher peaks correspond to the second ignition stage. The timing of this peak does not appear to change as a function of Reynolds number; although, a broader spread of this peak around the values shown for $Re = 5000$ is present at higher Reynolds numbers.

Based on the above observations, it would be interesting to see at what mixtures the various stages of autoignition occur. This will be investigated using conditional statistics of the temperature and the heat release rate.

Figures 18–20 show conditional statistics of temperature and heat release rate for case A, expressed in terms of the rate of change of temperature $-\frac{1}{\rho c_p} \sum_{k=1}^N h_k \dot{\omega}_k$ contributed by heat release, for times 0.15, 0.18, 0.21 and 0.24 s and corresponding to Reynolds numbers of 5000, 20,000 and 60,000, respectively. The conditioning is made based on the Bilger mixture fraction, which is expressed as [22]:

$$Z = \frac{2(Y_C - Y_{C,o})/W_C + (Y_H - Y_{H,o})/2W_H - (Y_O - Y_{O,o})/W_O}{2(Y_{C,f} - Y_{C,o})/W_C + (Y_{H,f} - Y_{H,o})/2W_H - (Y_{O,f} - Y_{O,o})/W_O} \quad (10)$$

where the Y 's are the elemental mass fractions corresponding to C, H and O; the W 's are atomic weights for C, H and O; and the subscripts

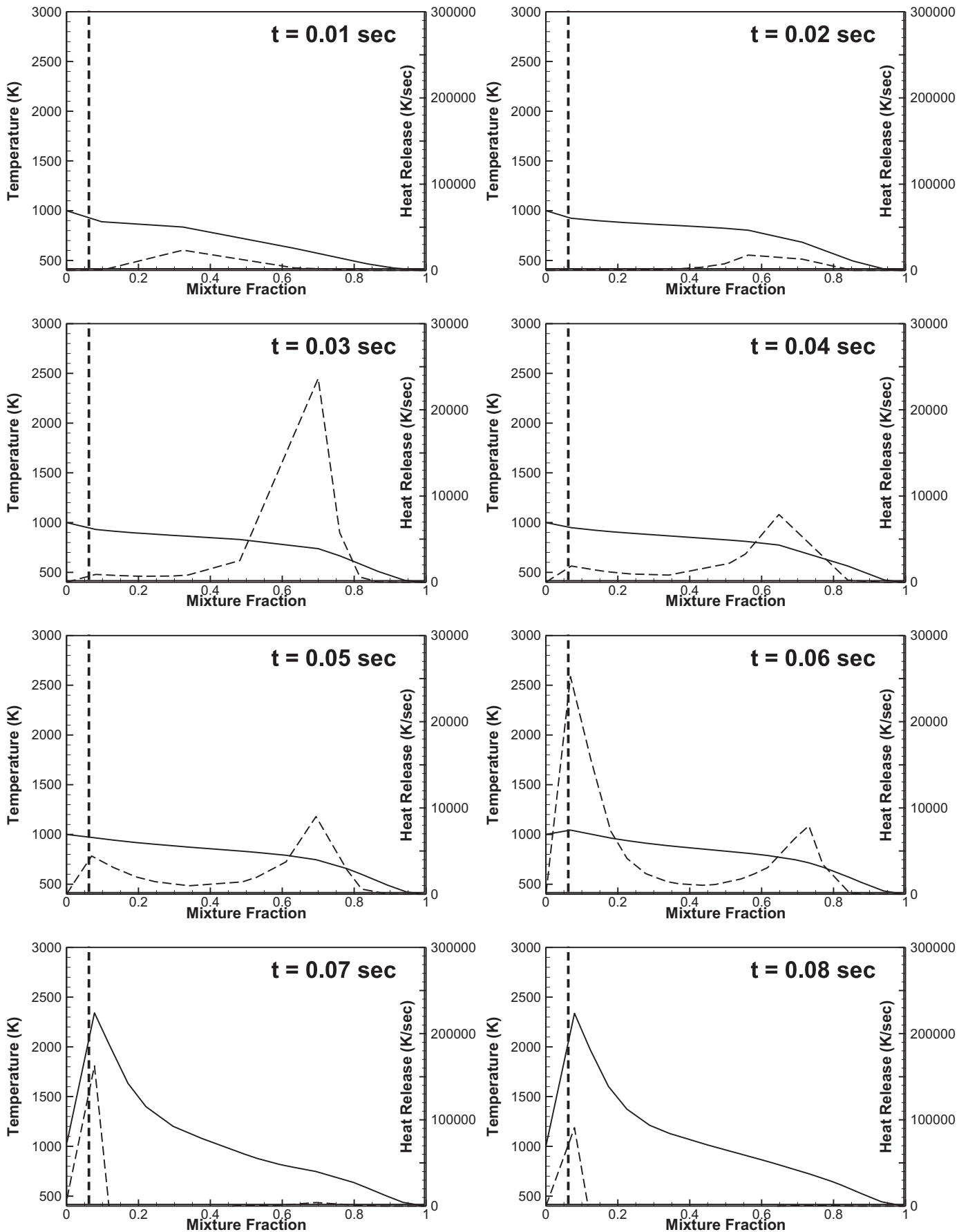


Fig. 21. Conditional means of temperature (solid) and heat release rate (dashed) for $Re = 5000$ and case B. The vertical dashed line corresponds to a stoichiometric mixture.

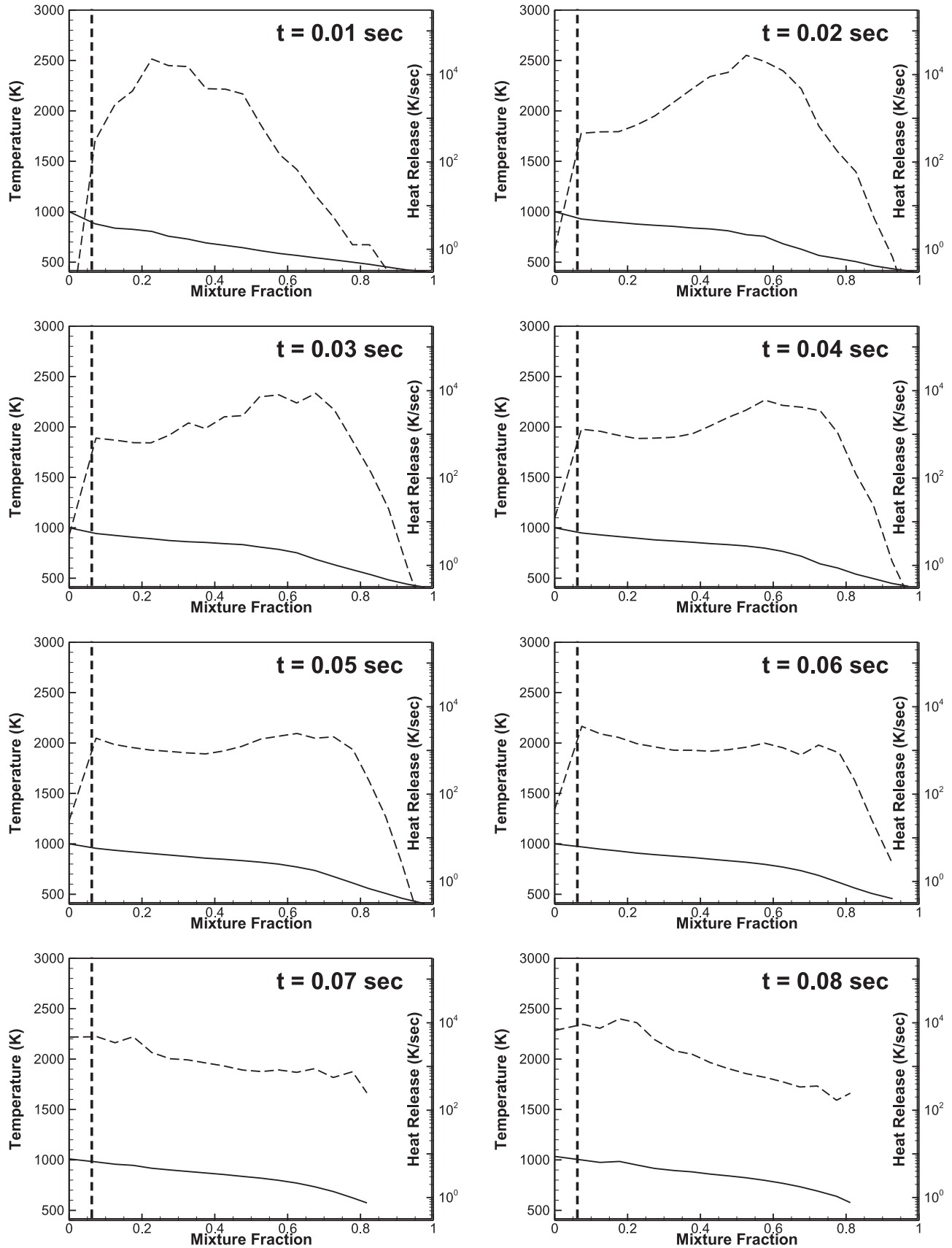


Fig. 22. Conditional means of temperature (solid) and heat release rate (dashed) for $Re = 20,000$ and case B. The vertical dashed line corresponds to a stoichiometric mixture.

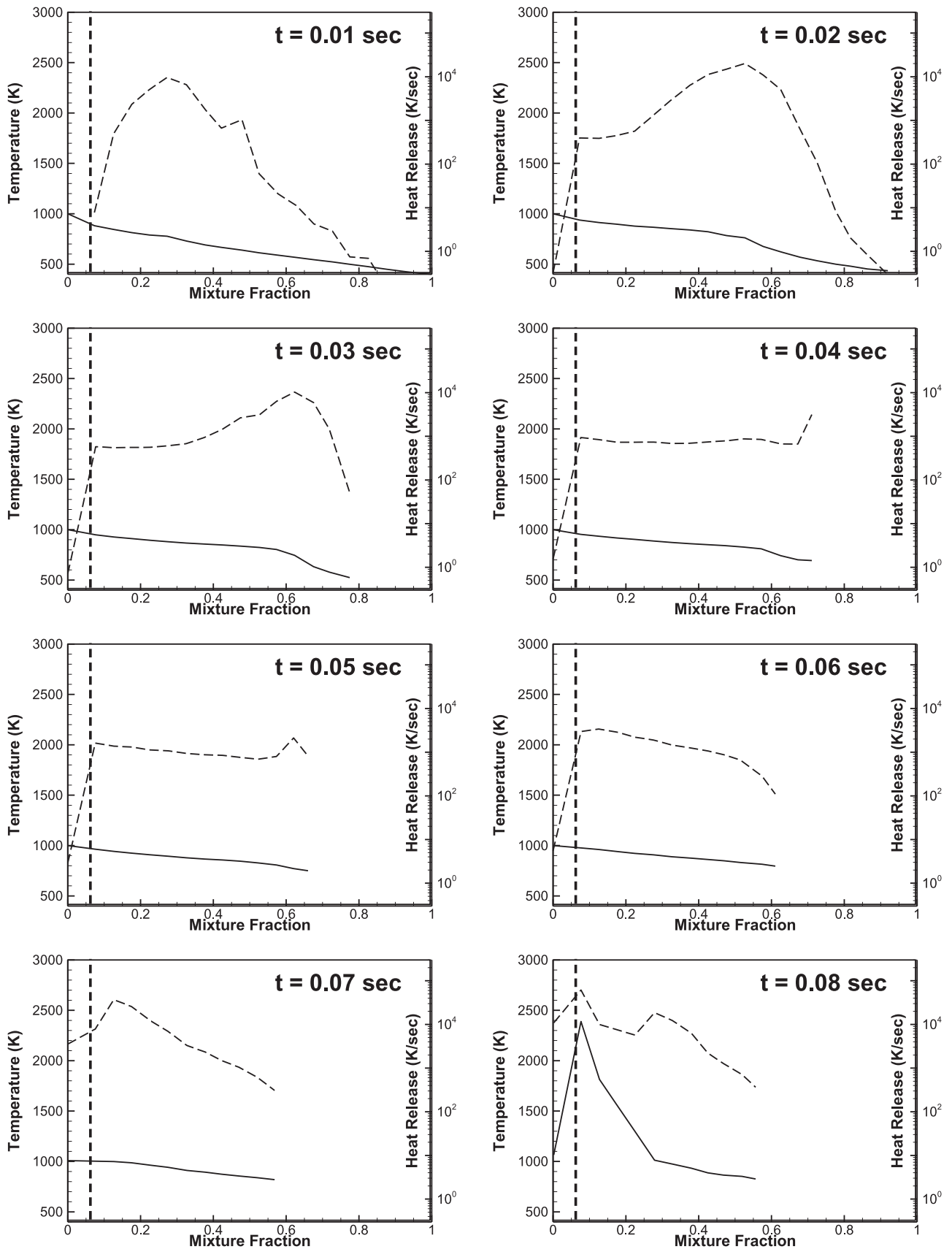


Fig. 23. Conditional means of temperature (solid) and heat release rate (dashed) for $Re = 60,000$ and case B. The vertical dashed line corresponds to a stoichiometric mixture.

f and o correspond to the reference conditions of the fuel jet and the coflow air, respectively. The statistics are based on 20 realizations of the ODT simulations of jet ignition for each case. The trends can be established even for as low as 5 realizations given the wide range of conditions encountered at a given realization.

The figures show that the earliest heat release occurs at leaner conditions; subsequently, the peak moves to richer conditions. The range of mixture fractions at the same times shrinks with the Reynolds number, indicating a process of mixing competing with that of reaction. Given that ignition delays are longer for case A, the time scales for turbulence compete directly with those associated with ignition delay.

Among the 3 Reynolds numbers shown for case A, the condition of $Re = 5000$ exhibits the earliest transition to autoignition. Compared to Fig. 7, which shows ignition delay times as a function of mixture fraction in the homogeneous case, it is clear that ignition propagation from leaner mixtures to richer mixtures precipitates the ignition process in rich mixtures.

Figures 21–23 show similar conditional statistics of temperature and heat release rate for case B for times 0.01, 0.02, 0.03, 0.04, 0.05, 0.06, 0.07 and 0.08 s and corresponding to Reynolds numbers of 5000, 20,000 and 60,000, respectively. The figures show that the earliest peaks of heat release rate do not occur at lean conditions where temperature is highest as in case A. Instead, they occur at rich conditions and correspond to the first-stage of ignition. These peaks initially migrate to even richer conditions (higher mixture fractions); then, a second peak forms at leaner mixtures, which is responsible for the most important temperature rise.

These observations illustrate the role of two-stage ignition of non-homogenous mixtures, like in the jet configuration studied here. The peaks that we observe as early as 0.01 s correspond to the onset of first-stage ignition at rich mixtures. We have to wait until 0.04 s to see the formation of a second peak at leaner mixtures. Meanwhile, as the leaner peak forms, the second peak at richer conditions continues to decay. By approximately this time, the two peaks are already in place, and are bridged by a range of lower values of the heat release. This range may or may not be a strong indication of an ignition front propagation from different mixtures as evidenced by observations of case A. However, an important consequence of the presence of first-stage ignition at rich conditions and the single-stage ignition at leaner mixtures is that the temperature profiles tend to be relatively flat in mixture fraction space. Accordingly, heat dissipation is reduced, further shielding nascent kernels from dissipation.

Figure 21 shows that for $Re = 5000$, the temperature rise above 1000 K occurs as early as 0.06 s, which is shorter than the shortest time reported for homogeneous mixtures. However, higher turbulence delays this temperature rise; although, the trend is not monotonic. For example, the case of $Re = 20,000$ shows the highest delay compared to 60,000. These trends may be interpreted as competition between higher turbulence conditions early on, which tend to increase scalar dissipation and delay the ignition process versus the formation of relatively shielded kernels with low dissipation at later times, which promotes ignition of neighboring layers.

5. Summary and conclusions

The autoignition of n-heptane/air mixtures in a co-flow jet configuration with preheated air and pre-vaporized fuel is investigated using the one-dimensional turbulence model. Different inlet jet Reynolds numbers and two conditions for air preheat are considered. The simulations are carried out with a 58-species reduced

mechanism and a detailed description of molecular transport. These simulations were augmented with homogeneous mixtures' simulations at different mixture conditions consistent with the preheated air and fuel reference states.

The simulations show that turbulence plays different and potentially competing roles for this fuel, which can be subjected to NTC effects. The first role is that scalar dissipation tends to delay ignition due to heat and radical losses from nascent kernels. However, once ignition is established, a rapid mixing of the mixture ensures much larger volumetric rates of heat release at conditions post-ignition.

Air preheat also plays an important role coupled with turbulence. As evidenced by the two air preheat temperature cases, the first ignition may occur at lean or rich mixtures and may correspond to the first-stage or the only stage of ignition. Beyond this initial stage, heat release from the mixture can play two different roles on the ignition of neighboring mixture layers. The first effect is that of ignition propagation, as shown in case A. The second effect translates into generating less temperature stratification enabling nascent kernels to experience lower heat dissipation. Both scenarios can precipitate the autoignition process at mixtures where further delay may be experienced at homogeneous conditions.

Acknowledgments

This paper was made possible by an NPRP award [NPRP 6-105-2-039] from the Qatar National Research Fund (a member of The Qatar Foundation). The statements made here are solely the responsibility of the authors. S.F. Ahmed would like to thank Qatar University for the support.

References

- [1] J.E. Dec, *SAE Trans.* 105 (1997) 119–139.
- [2] L.M. Pickett, D.L. Siebers, C.A. Idicheria, *SAE Paper 2005-01-3843* (2005). Society of Automotive Engineers.
- [3] R. Cabra, T. Myhrvold, J.-Y. Chen, R.W. Dibble, A.N. Karpetis, R.S. Barlow, *Proc. Combust. Inst.* 29 (2002) 1881–1888.
- [4] C.N. Markides, E. Mastorakos, *Proc. Combust. Inst.* 30 (2005) 883–891.
- [5] C.N. Markides, G. De Paola, E. Mastorakos, *Exp. Thermal Fluid Sci.* 31 (2007) 293–401.
- [6] T. Echehki, K. Gupta, *Int. J. Hydrogen Energy* 34 (2009) 8352–8377.
- [7] K. Gupta, T. Echehki, *Combust. Flame* 158 (2011) 327–344.
- [8] E. Mastorakos, T.A. Baritaud, T.J. Poinso, *Combust. Flame* 109 (1997) 198–223.
- [9] H.G. Im, J.H. Chen, C.K. Law, *Proc. Combust. Inst.* 27 (1998) 1047–1056.
- [10] R. Hilbert, D. Thévenin, *Combust. Flame* 128 (2002) 22–37.
- [11] T. Echehki, J.H. Chen, *Combust. Flame* 134 (2003) 169–191.
- [12] T. Echehki, A.R. Kerstein, T.D. Dreeben, J.-Y. Chen, *Combust. Flame* 125 (2001) 1083–1105.
- [13] C.S. Yoo, T.F. Lu, J.H. Chen, C.K. Law, *Combust. Flame* 158 (2011) 1727–1741.
- [14] H.J. Curran, P. Gaffuri, W.J. Pitz, C.K. Westbrook, *Combust. Flame* 129 (2002) 253–280.
- [15] A.E. Lutz, R.J. Kee, J.A. Miller, Sandia National Laboratories, SAND-87-8248 (1988).
- [16] M. Caracotsios, W.E. Stewart, *Comput. Chem. Eng.* 9 (1986) 359–365.
- [17] J.C. Hewson, A.R. Kerstein, *Combust. Theory Model.* 5 (2001) 669–697.
- [18] J.C. Hewson, A.R. Kerstein, *Combust. Sci. Technol.* 174 (2002) 35–66.
- [19] S. Zhang, T. Echehki, *Int. J. Hydrogen Energy* 33 (2008) 7295–7306.
- [20] B. Ranganath, T. Echehki, *Prog. Comput. Fluid Dyn.* 6 (2006) 409–418.
- [21] B. Ranganath, T. Echehki, *Combust. Sci. Technol.* 181 (2009) 597–617.
- [22] R.W. Bilger, S.H. Starner, R.J. Kee, *Combust. Flame* 80 (1990) 135–149.
- [23] P.N. Brown, G.D. Byrne, A.C. Hindmarsh, *SIAM J. Sci. Stat. Comput.* 10 (1989) 1038–1051.
- [24] R.J. Kee, J. Warnatz, J.A. Miller, Sandia National Laboratories Report SAND 83-8209; 1983.
- [25] R.J. Kee, J.A. Miller, T.H. Jefferson, Sandia National Laboratories Report SAND83-800; 1983.
- [26] P. Zhao, C.K. Law, *Combust. Flame* 160 (2013) 2352–2358.
- [27] J.A. van Oijen, *Proc. Combust. Inst.* 34 (2013) 1163–1171.
- [28] E. Oldenhof, M.J. Tummars, E.H. van Veen, D.J.E.M. Roekaerts, *Combust. Flame* 158 (2011) 1553–1563.
- [29] M.U. Göktolga, J.A. van Oijen, L.P.H. de Goey, Poster Presented at the 6th European Combustion Meeting, ECM, 25–28 June 2013, Lund, Sweden.